Fully Conjugated [4]Chrysaorene. Redox-Coupled Anion Binding in a Tetraradicaloid Macrocycle

Hanna Gregolińska,[†] Marcin Majewski,[†] Piotr J. Chmielewski,[†] Janusz Gregoliński,[†] Alan Chien,[‡] Jiawang Zhou,[||] Yi-Lin Wu,[||] Youn Jue Bae,[||] Michael R. Wasielewski,*[,||] Paul M. Zimmerman,*[,‡] and Marcin Stępień*[,†]

[†] Wydział Chemii, Uniwersytet Wrocławski, ul. F. Joliot-Curie 14, 50-383 Wrocław, Poland
[‡] Department of Chemistry, University of Michigan, 930 N. University Ave, Ann Arbor, MI 48109, USA
[||] Department of Chemistry and Institute for Sustainability and Energy at Northwestern, Northwestern University, Evanston IL 60208-3113

ABSTRACT: [4]Chrysaorene, a fully conjugated carbocyclic coronoid, is shown to be a low-bandgap π-conjugated system with a distinct open-shell character. The system shows good chemical stability and can be oxidized to well-defined radical cation and dication states. The cavity of [4]chrysaorene acts as an anion receptor towards halide ions with a particular selectivity toward iodides (K_a = 207 ± 6 M^{-1}). The interplay between anion binding and redox chemistry is demonstrated using a ^{1}H NMR analysis in solution. In particular, a well resolved, paramagnetically shifted spectrum of the [4]chrysaorene radical cation is observed, providing evidence for the inner binding of the iodide. The radical cation–iodide adduct can be generated in thin solid films of [4] chrysaorene by simple exposure to diiodine vapor.

INTRODUCTION

Coronoid aromatic molecules (cycloarenes) consist of a macrocycle enclosed by a fully fused periphery of π-conjugated rings.[1,2] Initially synthesized as models of annulene-within-annulene (AWA) aromaticity[3−5] and potential ligands,[6,7] coronoids have been more recently explored as curved aromatics,[8−11] graphene holes,[12] anion receptors,[10] and polyradicaloids.[13−15] In particular, octulene (**1**, Chart 1),[10] described in our recent report, was shown to possess a negatively curved surface and an unexpected ability to bind chloride anions in the macrocyclic cavity. While neutral C–H-bonding anion receptors had been known previously,[16−20] the anion-binding ability of **1** was unique because of the low polarity of its hydrogen-bond donors. Tetrahydro[4]chrysaorene (**2**), obtained in our earlier exploration of coronoid chemistry,[9,21] possesses a somewhat larger cavity than octulene, and we suspected that it might also act as an anion receptor. This was indeed confirmed in initial experiments; however, the incompletely conjugated structure of **2** and its relatively low stability made it of potentially lesser use as a receptor molecule.

We thus turned our attention to a fully conjugated analogue of **2**, the previously unknown [4]chrysaorene **3**, which we had anticipated to be a NIR-active chromophore with a possible open-shell character. In particular, the homology between **3** and Tobe's tetracyclopenta[*def*,*jkl*,*pqr*,*vwx*]tetraphenylene **4**[13] suggested a potentially tetraradicaloid nature of the [4]chrysaorene ring system. We reasoned that a larger number of Clar sextets in the tetraradicaloid configuration **3'** (eight vs. four in **4'**) may enhance the open-shell character of **3**. A substituted derivative of the [4]chrysaorene ring system, **3a**, was efficiently synthesized from the phenanthrene precursor **5**,[10] by using a peripheral stitching approach[14,15] (Scheme 1). **3a** was thoroughly characterized, revealing features characteristic of a uniquely small electronic bandgap and an open-shell electronic configuration. While our work was close to completion,[22] Wu et al. reported their concurrent research on **3a**, based on an essentially identical synthetic strategy.[23] The present account is therefore focused on the anion-binding capability of **3a** and its relationship to the redox chemistry of this open-shell coronoid.

Chart 1. π Conjugation in selected coronoid systems

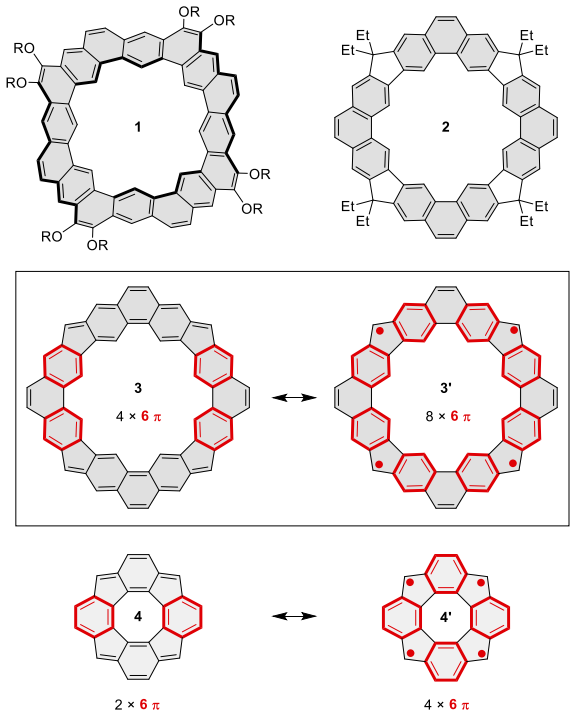

RESULTS AND DISCUSSION

Molecular and Electronic Structure. The molecular geometry of unsubstituted **3**, obtained in a broken-symmetry DFT optimization of the singlet state is shown in Figure 1. The diameter of the cavity in **3** is

6.12 Å, which is sufficiently large to accommodate the iodide anion. In octulene **1**, which also contains a 24-membered inner ring, the cavity is smaller (5.53–5.89 Å), because of the contraction caused by the hyperbolic distortion of the ring system.[10] DFT methods consistently represent **3** with a cyclically delocalized D_{4h}-symmetric geometry, analogous to that obtained previously for **4**.[13] However, in a multi-configurational geometry optimization, the latter system produced a localized bonding pattern, which agreed better with the solid-state geometry. Interestingly, **3** also gives a localized D_{2h}-symmetric geometry at the UNO-CASSCF(20,12)/6-311G(d,p) level of theory (Figure S4), even though the reported solid-state structure of **3a** appears to be closer to the fully delocalized form.[23] Accurate reproduction of bonding parameters remains a relevant problem in polyradicaloid chemistry, because the calculated orbital occupancies in such systems (and hence, radicaloid indexes) are strongly correlated with bond length delocalization. In the present case, spin-flip calculations[24] performed for the D_{4h}-symmetric CAM-B3LYP geometry of **3** at the RAS(4,4)-SF/cc-pvdz level of theory[25,26] produced di- and tetraradicaloid indices of $\gamma_0 = 1.00$ and $\gamma_1 = 0.62$, respectively, in good agreement with the values reported by the Wu team. RAS(4,4)-SF odd-electron densities obtained for the singlet and triplet states of **3** (Figure S19) show highest values at the outer carbons of five-membered rings, in line with the tetraradicaloid valence structure **3'**.

Scheme 1. Synthesis of a fully conjugated [4]chrysaorene[a] and selected resonance contributors.

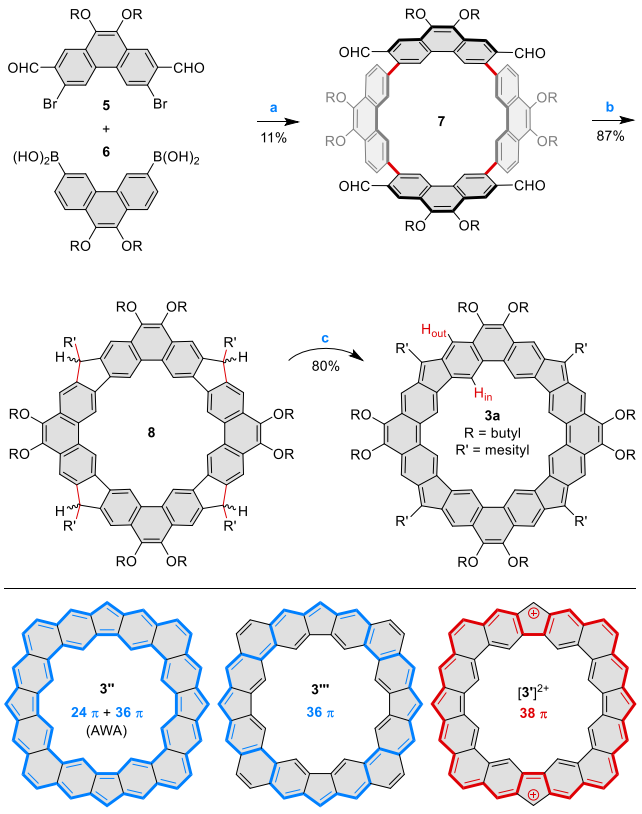

[a] Reagents and conditions: (a) $Pd(PPh_3)_4$ (20 mol %), dioxane, Na_2CO_3 (aq), reflux, overnight (b) 1. MesMgBr (10 equiv), THF, rt, overnight; 2. $BF_3{\cdot}Et_2O$, DCM, 5 min. (c) 1. DDQ (5 equiv), toluene, rt, 2 h; 2. KO_2 (24 equiv), DCM, 2 h.

Temperature-dependent broadening of ^{1}H NMR spectra is observed for many open-shell singlet systems, and is attributable to rapid exchange with a thermally populated triplet state. Accordingly, the ^{1}H NMR spectrum of the neutral **3a** was reported to be severely broadened in THF-d_8, and the H_{in} and H_{out} signals of the macrocycle (Scheme 1) could not be identified even at 193 K.[23] However, we found that a complete resonance pattern could be observed for **3a** at low temperatures in $CDCl_3$, CD_2Cl_2, toluene-d_8, and in mixtures of these solvents. The spectrum becomes reasonably sharp below 220 K, indicating that **3a** indeed exists as a diamagnetic species in its ground state (Figure 2). At 200 K in a 9:1 toluene-d_8–$CDCl_3$ mixture, the inner macrocycle protons (H_{in}) of **3a** yielded a low-field signal at 18.91 ppm. The latter shift is much larger than expected in the case of benzenoid (Clar-type) conjugation,[3,4,9,10] indicating a potentially paratropic character of the macrocycle. This property of **3a** is confirmed by the markedly upfield shifts of the outer protons (H_{out}) at the [4]chrysaorene ring system (3.93 ppm) and of the substituents (e.g., 1.98 ppm for *o*-Me and 2.78 for α-CH_2 of the Mes and Bu groups, respectively).

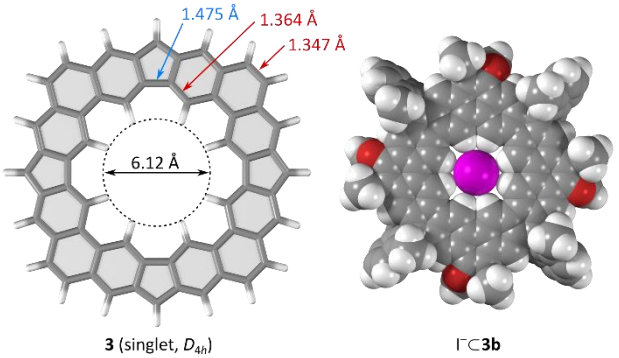

Figure 1. Molecular geometries of **3** (left, bs-UCAM-B3LYP/6-311++G(d,p)) and $I^-\subset$[**3b**] (right, R = Me, R' = 2,6-dimethylphenyl, bs-UωB97XD/6-31G(d,p)-SDD). In each case an open-shell singlet state was optimized. Partially localized single and double bonds in **3** are indicated in blue and red, respectively.

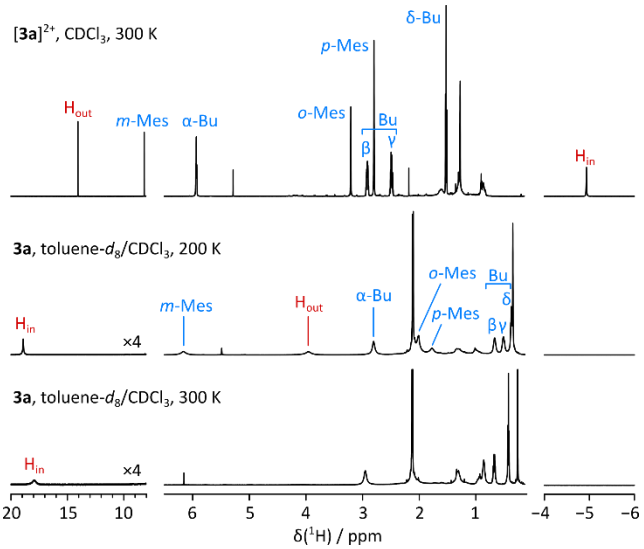

Figure 2. 600 MHz ^{1}H NMR spectra of **3a** and [**3a**]$^{2+}$. The dication was generated by treatment with excess Br_2.

The macrocyclic paratropicity of **3a** could at first sight be rationalized in terms of an AWA conjugation consisting of 24- and 36-electron pathways (**3''**, Scheme 1). However, the lengths of radial C–C bonds in both the experimental and calculated geometries of [4]chrysaorene (typically 1.43 to 1.44 Å) indicate that the outer and inner circuits in **3** are not fully decoupled. Furthermore, the ring current in **3a** is apparently much

stronger than in [24]annulene, for which the inner protons were found to resonate at 12.08 and 12.66 ppm.[27] The paratropicity is more likely to originate from [36]annulenoid pathways such as **3'''**, which (a) do not imply complete AWA decoupling and (b) agree with the observed partial localization of double bonds outside the path (Figure 1). Importantly, **3'''** and similar paths can be constructed by employing the same set of canonical structures that is used in the closed-shell benzenoid formulation **3** (see Scheme S6). This feature enables coexistence of benzenoid and macrocyclic conjugation, analogous to that previously observed in phenylene-containing porphyrinoids.[28]

Neutral Anion Receptor. In spite of its smaller electronic bandgap and non-negligible open-shell character, [4]chrysaorene **3a** is significantly more stable in solution than the tetrahydro prototype **2**. This remarkable feature provides an opportunity to study anion-binding interactions of a polyradicaloid structure. Since the low charge density of the iodide anion makes appropriate receptors difficult to design,[29–34] the use of **3a** for iodide binding was considered of particular interest. Receptor properties of **3a** were initially explored using ^{1}H NMR spectroscopy under slow-exchange conditions (9:1 toluene-d_8–$CDCl_3$ solvent mixture, 220 K). Upon addition of tetrabutylammonium iodide (TBAI), the $I^-\subset$**3a** adduct was indeed observed (Scheme 2), with the H_{in} signal at ca. 20.7 ppm (vs. 18.58 ppm for the free **3a**). However, strong ion pairing of $I^-\subset$**3a** with the ammonium counter-cation, inferred from extensive broadening of TBA signals, made it difficult to quantitatively analyze the anion-binding equilibrium. The anion–[4]chrysaorene interaction was however sufficiently strong in a more polar medium (CD_2Cl_2, 300 K) to permit determination of binding parameters in the fast exchange limit (Figures S13–15). The I^- binding constant K_a established for **3a** was 207 ± 6 M^{-1}, higher than for a recently reported cyclocarbazole receptor (82 ± 9 M^{-1}).[33] **3a** shows considerable selectivity towards the iodide, with significantly lower K_a values determined for Br^- and Cl^- (61 ± 7 and 2.4 ± 0.8 M^{-1}, respectively). Face-to-face aggregated 1:2 adducts, $X^-\subset$[**3a**]$_2$, analogous to those observed for some triazolophane receptors,[35,16] are not expected to form, because of the steric bulk of Mes substituents and the conformational rigidity of the chrysaroene ring.

Scheme 2. Anion-binding and redox equilibria of [4]chrysaorene 3a.

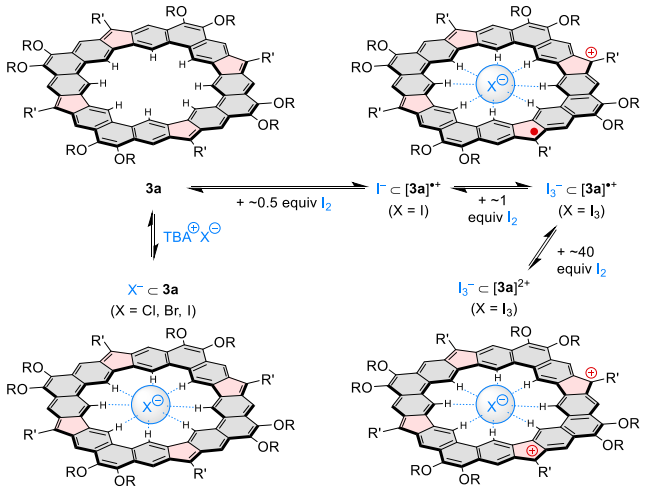

Oxidized States and Their Properties. Cyclic voltammetry performed for **3a** in dichloromethane showed three oxidations (–0.18 V, –0.13 V, and 0.64 V vs. Fc^+/Fc) and four reductions (one two-electron event at –1.26 V and two one-electron events at –1.75 and –1.95 V, Figure S1). These values correspond to a very small electronic bandgap of 1.08 V, in line with the extended NIR absorption of the [4]chrysaorene chromophore. The two lowest, closely spaced oxidations appear below the oxidation potential of Br_2 (ca. 0.07 V, in acetonitrile[36]) and are in fact very close to the potential of I_2 (–0.14 V). We thus envisaged that, by using the above two mild reagents, it might be possible to combine oxidation of the [4]chrysaorene ring with halide anion binding. This aspect was of additional interest because of the capacity of anion binding to affect the oxidation levels of redox-active receptors.[37–39]

In initial experiments, it was found that when solutions of **3a** were treated with Br_2 vapors, the compound was cleanly converted into the dicationic form [**3a**]$^{2+}$. Similar results were obtained with a stoichiometric amount of 2,3-dichloro-5,6-dicyano-1,4-benzoquinone (DDQ). The ^{1}H NMR spectrum of [**3a**]$^{2+}$ (Figure 2) reveals a strong macrocyclic diatropic ring current, manifested by the respectively upfield an downfield shifts of the H_{in} and H_{out} protons of the [4]chrysaorene ring (–4.94 and 14.04 ppm), comparable with values recorded for similarly sized expanded porphyrinoids (see ref. [37] for a representative example). Unlike the neutral **3a**, the [**3a**]$^{2+}$ dication displays narrow lines in its room-temperature ^{1}H NMR spectrum, consistent with a fully diamagnetic structure. Consequently, complete assignment of the ^{1}H and ^{13}C NMR signals was achieved with the aid of 2D spectroscopy and GIAO calculations (Scheme S5, Figures S2–S3). The observed macrocyclic aromaticity of [**3a**]$^{2+}$ can be rationalized in terms of 38-electron circuits, such as [**3'**]$^{2+}$ (Scheme 1). This type of conjugation should place a considerable fraction of the positive charge on the Mes-substituted carbons of the five-membered rings in [**3a**]$^{2+}$. In support of this hypothesis, the corresponding position produces the most downfield ^{13}C shift (167.2 ppm), in line with the expected partial carbocationic character of this site.

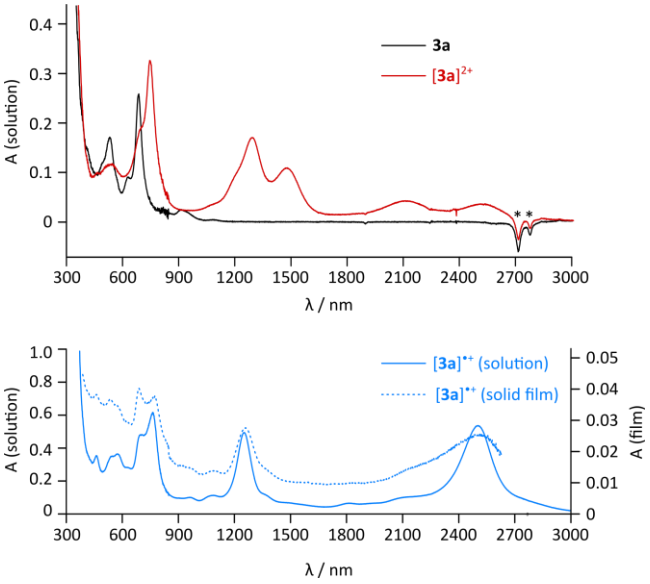

Figure 3. Top: electronic absorption spectra (in CD_2Cl_2) of **3a** and [**3a**]$^{2+}$ (obtained by addition of DDQ). Negative peaks at in the 2700–2800 nm range are due to an imperfect baseline subtraction. Bottom: electronic absorption spectra of [**3a**]$^{\bullet+}$ generated by addition of ca. 0.5 equiv I_2 to a $CDCl_3$ solution of **3a** (solid line), and by exposure of a thin film of **3a** to I_2 vapor (dotted line; after 2 days at ambient conditions).

The Br_2 oxidation occurs in two steps, with accurate isosbestic points observed at the initial titration stage. The intermediate species, presumed to be the radical cation [**3a**]$^{\bullet+}$, shows a significantly reduced optical bandgap relative to the neutral **3a**, similarly to the dicationic species (Figure 3). [**3a**]$^{\bullet+}$ could be generated with greater precision using I_2 vapors. The formation of a radical species was additionally confirmed by

ESR spectroscopy, which showed a significant increase of signal intensity, when a DCM solution of **3a** was treated with I_2 (Figure S#). In subsequent titration experiments, it was found that ca. 0.5 equiv of diiodine is needed to effect complete one-electron oxidation, in agreement with the formal stoichiometry of the reaction, whereas a much larger excess is necessary (> 40 equiv) to obtain complete conversion to the dication. Interestingly, when a thin film of neat **3a** is exposed to iodine vapors, the material is immediately oxidized to a mixture of $[\mathbf{3a}]^{\bullet+}$ and $[\mathbf{3a}]^{2+}$, as inferred from the absorption spectrum (Figure S18). The oxidation is partly reverted when the sample is left in air for several hours, to produce a spectrum corresponding to that of pure $[\mathbf{3a}]^{\bullet+}$ (Figure 3). Such films remain stable for several days when stored under ambient conditions.

Femtosecond transient absorption (TA) spectra recorded for neutral **3a** (Figures 4 and S7–10) revealed a biexponential decay in $CDCl_3$. The data were best fit to an A → B → GS first-order kinetic model with time constants of 0.7 and 15.7 ps (GS = ground state). In this solvent, photoinduced oxidation produced small amounts of the radical cation $[\mathbf{3a}]^{\bullet+}$, an effect that was absent in CD_2Cl_2. A similar TA behavior was observed for $[\mathbf{3a}]^{\bullet+}$ (0.5 and 14.3 ps) and $[\mathbf{3a}]^{2+}$ (1.4 and 13.0 ps), generated in situ by addition of I_2 and Br_2, respectively. For all three samples, photoexcitation with 710-nm pulses first populates the first excited state (species A), which shows strong excited-state absorption in the near-IR region and undergoes rapid deactivation (~ 1 ps) to generate species B. The species-associated spectra (SAS) of B, displaying positive TA signals slightly lower in energy relative to each of the GS absorbance features, suggest the formation of a hot ground state (^{hot}GS). This rapid electronic deactivation behavior is apparently related to the small energy gap in **3a** and its oxidized states, characteristic of open-shell and π-extended aromatics;[40] it can also result from the conversion through a conical intersection between the first excited state and the ground state.[41]

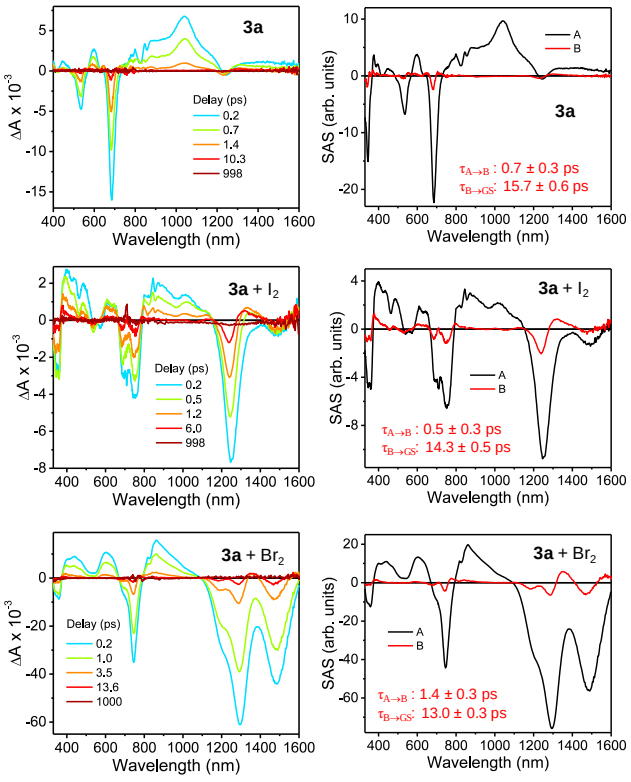

Figure 4. Femtosecond transient absorption (fs-TA) spectra (left) and species-associated spectra (right) for **3a** and its radical cation and dication, obtained respectively by reaction with diiodine and dibromine ($CDCl_3$ solvent, 710 nm excitation wavelength). TA decay profiles are given in the Supporting Information.

Redox Chemistry vs. Anion Binding. To gain further insight into the above oxidation process, we titrated **3a** with a solution of diiodine under ^{1}H NMR control (Figure 5, Scheme 2). At 300 K, during the addition of the first 0.5 equiv of I_2, a new species emerged, characterized by a very unusual set of signals. In particular, a very broad resonance ($\nu_{1/2}$ ~380 Hz) was initially observed at 46.1 ppm. These parameters suggested that the new form is paramagnetic and that the radical cation $[\mathbf{3a}]^{\bullet+}$ is actually being observed. In support of this assumption, the above signal gave a near-perfect Curie dependence in the 330–210 K range, extrapolating to 13.00 ppm in the diamagnetic limit (Figure S5). In spite of its broadness, this resonance could be unequivocally assigned to the H_{in} protons of the macrocycle, using the ^{1}H EXSY pattern observable between signals of $[\mathbf{3a}]^{\bullet+}$ and **3a** (Figure S12). On the same basis, a set of upfield signals in the 0 to −2 ppm range were assigned to the peripheral butyl chains. The unusual sequence of shifts ($\delta_\alpha > \delta_\delta > \delta_\beta > \delta_\gamma$) is likely indicative of through-bond transfer of spin density to the butyl chain.

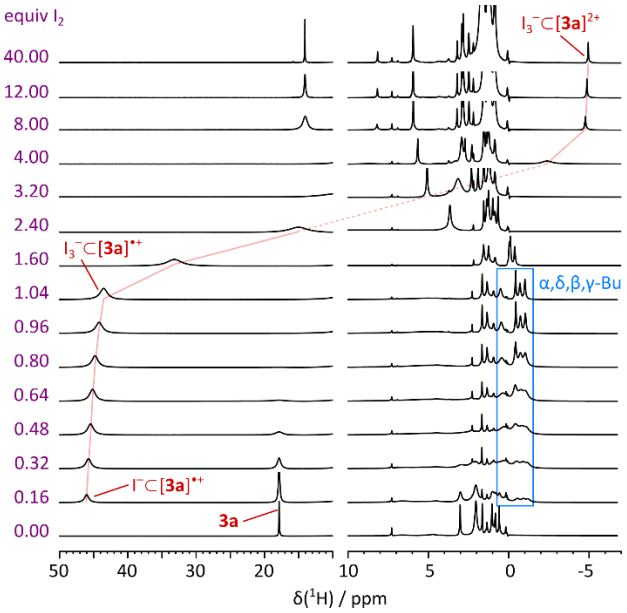

Figure 5. Titration of **3a** with diiodine monitored using ^{1}H NMR spectroscopy ($CDCl_3$, 300 K, 600 MHz, durene as internal reference). Signals of the inner protons (H_{in}) are labeled in red. Relative scaling of individual traces has been adjusted to improve readability.

The fate of iodide ions released in the course of the oxidation process can be inferred from the NMR spectra. $[\mathbf{3a}]^{\bullet+}$ and **3a** are observed in equilibrium (and in slow exchange) up to ca. 0.8 equiv of added I_2. Importantly, at this stage of the titration, the H_{in} chemical shift of neutral **3a** remains constant. Since iodide binding in the cavity of [4]chrysaorene results in a downfield relocation of the H_{in} resonance (*vide supra*), it can be concluded the iodide complex $I^-\subset\mathbf{3a}$ is not formed during the I_2 titration. This observation is explained by assuming competitive iodide binding by the radical cation $[\mathbf{3a}]^{\bullet+}$. The resulting inclusion complex $I^-\subset[\mathbf{3a}]^{\bullet+}$ is formed with a much higher binding constant than $I^-\subset\mathbf{3a}$, thus consuming most of the available iodide. The greater stability of $I^-\subset[\mathbf{3a}]^{\bullet+}$ likely originates from the electrostatic interaction between the two ions, and may be further enhanced by the more favorable solvation of the neutral ion pair. Geometrical factors may also play a

secondary role: DFT calculations predict a D_{2h}-symmetric structure for the unsubstituted $[\mathbf{3}]^{\bullet+}$, consistent with a weak Jahn–Teller distortion (Figure S4).[42,43] In consequence, the inner cavity of $[\mathbf{3}]^{\bullet+}$ takes a slightly elongated shape and is somewhat smaller than the receptor site in the neutral **3** (diagonal H···H distances of 6.05–6.10 Å).

The ^{1}H NMR spectral pattern of $[\mathbf{3a}]^{\bullet+}$ is observable up to ca. 1 equiv of added I_2. In that titration range, shifts and linewidths undergo subtle changes (Figure S6), indicating that an additional process may be occurring in the presence of excess diiodine (> 0.5 equiv). The H_{in} signal moves gradually to higher field (from ca. 46 to 43 ppm), while its linewidth increases, with an inflection point at ca. 0.6 equiv. A more pronounced effect is seen for the signals of the butyl chain (blue box, Figure 5), which become much sharper above 0.6 equiv I_2 and move slightly upfield. It is presumed that the excess diiodine reacts with the complexed iodide, to produce a new ion pair, $I_3^-\subset[\mathbf{3a}]^{\bullet+}$. Under our experimental conditions, the exchange between $I^-\subset[\mathbf{3a}]^{\bullet+}$ and $I_3^-\subset[\mathbf{3a}]^{\bullet+}$ was fast, and the two species yielded an averaged set of resonances.

Interactions of triiodide with macrocyclic receptors are often relatively weak, and I_3^- is frequently found outside the cavity in solid-state structures.[44,39] However, even though the triiodide anion is significantly larger than I^-, its oblong shape is expected to facilitate binding in the cavity of $[\mathbf{3a}]^{\bullet+}$. Non-bonded C–H···I contacts observed in the solid state for terminal atoms of I_3^- (~3.1 Å) are comparable with the cavity radius of [4]chrysaorene.[45] In a DFT model of $I_3^-\subset[\mathbf{3}]^{\bullet+}$ (Figure S21), the triiodide is recessed into the cavity by only ca. 1.4 Å. In consequence the proximal I–I bond becomes longer than the distal bond, a feature typically observed in asymmetrically bound triiodides.

The composition of the $I_3^-\subset[\mathbf{3a}]^{\bullet+}$ complex corresponds to 1.5 equiv of added I_2, and complete conversion into this ion pair might be expected at or above this equivalent ratio. However, upon addition of a larger excess of diiodine, the ^{1}H NMR spectrum undergoes a drastic change, and a spectral pattern corresponding to the aromatic dication $[\mathbf{3a}]^{2+}$ eventually emerges, in agreement with the spectrophotometric observations. As the radical cation and dicationic forms are in fast exchange, the H_{in} signal is observed to travel across the entire spectral range, from ca. +45 ppm to −5 ppm.

^{1}H NMR spectra of organic radicals, such as $[\mathbf{3a}]^{\bullet+}$, are typically difficult to observe because of severe line broadening, which is dependent on the electronic relaxation rate and on spin densities on respective protons.[46–49] To confirm the anion-binding effect on the observed NMR dynamics, we performed a reference oxidation experiment in the presence of a bulky, non-binding counteranion $[SbF_6]^-$ (Figure S16). We observed a qualitatively similar, two-step oxidation behavior; however, in the absence of iodide anions, the inner protons of $[\mathbf{3a}]^{\bullet+}$ yielded a much broader signal ($\nu_{1/2}$ ~2.8 kHz), which would be difficult to interpret without reference to the I_2 titration data discussed above. It is presumed that the binding of I^-/I_3^- in the cavity of [4]chrysaorene, may enhance electronic relaxation in $[\mathbf{3a}]^{\bullet+}$, thus leading to much narrower resonances of the $I_n^-\subset[\mathbf{3a}]^{\bullet+}$ complexes. The corresponding H_{in} signal of **3a** was also more broadened (though to a lesser extent), when **3a** and $[\mathbf{3a}]^{\bullet+}$ were observed simultaneously in equilibrium. Furthermore, a dynamically averaged set of Bu signals was observed for **3a** and $[\mathbf{3a}]^{\bullet+}$ in the presence of the non-binding $[SbF_6]^-$ anion, indicating that the chemical exchange between the two species is faster than in the diiodine-oxidized sample. Because of the much larger shift difference (ca. 27 ppm or 16 kHz), **3a** and $[\mathbf{3a}]^{\bullet+}$ yielded separate H_{in} resonances characteristic of the slow-exchange regime, yet the broadening of the **3a** resonance, greater than in the I_2 oxidation experiment, is attributable to faster exchange dynamics. The slower $\mathbf{3a} \rightleftharpoons I_n^-\subset[\mathbf{3a}]^{\bullet+}$ exchange observed during the I_2 oxidation may indicate that the process is rate-limited by the dissociation of the I^-/I_3^- anion from the $[\mathbf{3a}]^{\bullet+}$ receptor site. An intermediate case of line broadening was observed when **3a** was titrated with dibromine (Figure S17), in agreement with the expected weaker binding of the bromide anion in the cavity of $[\mathbf{3a}]^{\bullet+}$.

CONCLUSIONS

[4]Chrysaorene combines reversible multi-redox behavior with anion-binding ability to permit an unprecedented observation of interactions between anions and different oxidation levels of a heteroatom-free macrocycle. The non-polar cavity of **3a** is a surprisingly good receptor for iodide anions, benefiting from the rigid conformation and precise match between the cavity and the ionic radius of I^-. Stabilization of such a host–guest interaction in an all-carbon macrocycle with no inner functional groups is still a rare phenomenon,[10,33,50] which appears to be of a mostly dispersive character. The increased electrostatic component provides for an even stronger interaction between the iodide and the radical cation of [4]chrysaorene, resulting in a complete transfer of the anion into the more charged cavity upon oxidation.

Neutral π-aromatic radicals are typically designed on the basis of inherently odd-electron frameworks, or the overall charge is adjusted by metal coordination in macrocyclic systems.[51] $I_n^-\subset[\mathbf{3a}]^{\bullet+}$ adducts are different in this regard, because the charge is being compensated by inclusion of an anion, in analogy to some closed-shell porphyrinoids.[52,53] More generally, the formation of such inclusion complexes in the solid state may provide access to potentially highly conductive low-bandgap materials. Efforts to explore this potential are currently underway in our laboratories.

ASSOCIATED CONTENT

Supporting Information

Synthetic and spectroscopic details, computational data. The Supporting Information is available free of charge on the ACS Publications website.

AUTHOR INFORMATION

Corresponding Author

m-wasielewski@northwestern.edu
paulzim@umich.edu
marcin.stepien@chem.uni.wroc.pl

ACKNOWLEDGMENT

The project was funded by the National Science Centre of Poland (DEC-2012/07/E/ST5/00781 to M.S. and DEC-2015/19/N/ST5/00760 to M.A.M.). P. M. Z. thanks the Alfred P. Sloan Foundation for support of this project. The work at Northwestern University was supported by the U.S. Department of Energy, Office of Science, Office of Basic Energy Sciences under Award DE-FG02-99ER14999 (M.R.W.). Quantum-chemical calculations were performed in the Wrocław Center for Networking and Supercomputing.

REFERENCES

(1) Miyoshi, H.; Nobusue, S.; Shimizu, A.; Tobe, Y. Non-Alternant Non-Benzenoid Kekulenes: The Birth of a New Kekulene Family. *Chem. Soc. Rev.* **2015**, *44* (18), 6560–6577.

(2) Buttrick, J. C.; King, B. T. Kekulenes, Cycloarenes, and Heterocycloarenes: Addressing Electronic Structure and Aromaticity through Experiments and Calculations. *Chem. Soc. Rev.* **2017**, *46* (1), 7–20.

(3) Diederich, F.; Staab, H. A. Benzenoid versus Annulenoid Aromaticity: Synthesis and Properties of Kekulene. *Angew. Chem. Int. Ed. Engl.* **1978**, *17* (5), 372–374.

(4) Kumar, B.; Viboh, R. L.; Bonifacio, M. C.; Thompson, W. B.; Buttrick, J. C.; Westlake, B. C.; Kim, M.-S.; Zoellner, R. W.; Varganov, S. A.; Mörschel, P.; Teteruk, J.; Schmidt, M. U.; King, B. T. Septulene: The Heptagonal Homologue of Kekulene. *Angew. Chem. Int. Ed.* **2012**, *51* (51), 12795–12800.

(5) Stępień, M. An Aromatic Riddle: Decoupling Annulene Conjugation in Coronoid Macrocycles. *Chem* **2018**, *4* (7), 1481–1483.

(6) Bell, T. W.; Cragg, P. J.; Drew, M. G. B.; Firestone, A.; Kwok, A. D.-I.; Liu, J.; Ludwig, R. T.; Papoulis, A. T. Synthesis of New Torands and New Uses for Old Torands. *Pure Appl. Chem.* **1993**, *65* (3), 361–366.

(7) Tatibouët, A.; Hancock, R.; Demeunynck, M.; Lhomme, J. Synthesis of 3,9,15,19,21,23-Hexaazakekulene. *Angew. Chem. Int. Ed. Engl.* **1997**, *36* (11), 1190–1191.

(8) Myśliwiec, D.; Stępień, M. The Fold-In Approach to Bowl-Shaped Aromatic Compounds: Synthesis of Chrysaoroles. *Angew. Chem. Int. Ed.* **2013**, *52* (6), 1713–1717.

(9) Majewski, M. A.; Lis, T.; Cybińska, J.; Stępień, M. Chrysaorenes: Assembling Coronoid Hydrocarbons via the Fold-in Synthesis. *Chem. Commun.* **2015**, *51* (82), 15094–15097.

(10) Majewski, M. A.; Hong, Y.; Lis, T.; Gregoliński, J.; Chmielewski, P. J.; Cybińska, J.; Kim, D.; Stępień, M. Octulene: A Hyperbolic Molecular Belt That Binds Chloride Anions. *Angew. Chem. Int. Ed.* **2016**, *55* (45), 14072–14076.

(11) Yang, Y.; Chu, M.; Miao, Q. From Phenanthrylene Butadiynylene Macrocycles to S-Heterocycloarenes. *Org. Lett.* **2018**, *20* (14), 4259–4262.

(12) Beser, U.; Kastler, M.; Maghsoumi, A.; Wagner, M.; Castiglioni, C.; Tommasini, M.; Narita, A.; Feng, X.; Müllen, K. A C216-Nanographene Molecule with Defined Cavity as Extended Coronoid. *J. Am. Chem. Soc.* **2016**, *138* (13), 4322–4325.

(13) Nobusue, S.; Miyoshi, H.; Shimizu, A.; Hisaki, I.; Fukuda, K.; Nakano, M.; Tobe, Y. Tetracyclopenta[Def,Jkl,Pqr,Vwx]Tetraphenylene: A Potential Tetraradicaloid Hydrocarbon. *Angew. Chem. Int. Ed.* **2015**, *54* (7), 2090–2094.

(14) Das, S.; Herng, T. S.; Zafra, J. L.; Burrezo, P. M.; Kitano, M.; Ishida, M.; Gopalakrishna, T. Y.; Hu, P.; Osuka, A.; Casado, J.; Ding, J.; Casanova, D.; Wu, J. Fully Fused Quinoidal/Aromatic Carbazole Macrocycles with Poly-Radical Characters. *J. Am. Chem. Soc.* **2016**, *138* (24), 7782–7790.

(15) Liu, C.; Sandoval-Salinas, M. E.; Hong, Y.; Gopalakrishna, T. Y.; Phan, H.; Aratani, N.; Herng, T. S.; Ding, J.; Yamada, H.; Kim, D.; Casanova, D.; Wu, J. Macrocyclic Polyradicaloids with Unusual Super-Ring Structure and Global Aromaticity. *Chem* **2018**, *4* (7), 1586–1595.

(16) Flood, A. H. Creating Molecular Macrocycles for Anion Recognition. *Beilstein J. Org. Chem.* **2016**, *12*, 611–627.

(17) Farnham, W. B.; Roe, D. C.; Dixon, D. A.; Calabrese, J. C.; Harlow, R. L. Fluorinated Macrocyclic Ethers as Fluoride Ion Hosts. Novel Structures and Dynamic Properties. *J. Am. Chem. Soc.* **1990**, *112* (21), 7707–7718.

(18) Zhu, S. S.; Staats, H.; Brandhorst, K.; Grunenberg, J.; Gruppi, F.; Dalcanale, E.; Lützen, A.; Rissanen, K.; Schalley, C. A. Anion Binding to Resorcinarene-Based Cavitands: The Importance of C–H···Anion Interactions. *Angew. Chem. Int. Ed.* **2008**, *47* (4), 788–792.

(19) Li, Y.; Flood, A. H. Pure C–H Hydrogen Bonding to Chloride Ions: A Preorganized and Rigid Macrocyclic Receptor. *Angew. Chem. Int. Ed.* **2008**, *47* (14), 2649–2652.

(20) Lee, S.; Chen, C.-H.; Flood, A. H. A Pentagonal Cyanostar Macrocycle with Cyanostilbene CH Donors Binds Anions and Forms Dialkylphosphate [3]Rotaxanes. *Nat. Chem.* **2013**, *5* (8), 704–710.

(21) In the original paper, the trivial name [4]chrysaorene was used for the tetrahydro species. Since the organic nomenclature requires that base names for ring systems refer to fully dehydrogenated structures, we now correct the naming system accordingly.

(22) Stępień, M. From Coronoid Macrocyles to Stable Biradicaloid Systems. In *German-Polish-Baltic Conference on Organic Chemistry. Hamburg, 15th-19th May 2018, Book of Abstracts*; Hamburg–Blankenese, 2018.

(23) Lu, X.; Gopalakrishna, T. Y.; Phan, H.; Herng, T. S.; Jiang, Q.; Liu, C.; Li, G.; Ding, J.; Wu, J. Global Aromaticity in Macrocyclic Cyclopenta-Fused Tetraphenanthrenylene Tetraradicaloid and Its Charged Species. *Angew. Chem. Int. Ed.* **2018**, *57* (40), 13052–13056.

(24) Krylov, A. I. Size-Consistent Wave Functions for Bond-Breaking: The Equation-of-Motion Spin-Flip Model. *Chem. Phys. Lett.* **2001**, *338* (4), 375–384.

(25) Zimmerman, P. M.; Bell, F.; Goldey, M.; Bell, A. T.; Head-Gordon, M. Restricted Active Space Spin-Flip Configuration Interaction: Theory and Examples for Multiple Spin Flips with Odd Numbers of Electrons. *J. Chem. Phys.* **2012**, *137* (16), 164110.

(26) Bell, F.; Zimmerman, P. M.; Casanova, D.; Goldey, M.; Head-Gordon, M. Restricted Active Space Spin-Flip (RAS-SF) with Arbitrary Number of Spin-Flips. *Phys. Chem. Chem. Phys.* **2013**, *15* (1), 358–366.

(27) Oth, J. F. M.; Zélicourt, Y. de J. de. Mobilité Conformationnelle et Migration Des Liaisons π Dans Le [24]Annulène. *Helv. Chim. Acta* **1999**, *82* (3), 435–483.

(28) Stępień, M.; Latos-Grażyński, L. Tetraphenyl-p-Benziporphyrin: A Carbaporphyrinoid with Two Linked Carbon Atoms in the Coordination Core. *J. Am. Chem. Soc.* **2002**, *124* (15), 3838–3839.

(29) Singh, N.; Jang, D. O. Benzimidazole-Based Tripodal Receptor: Highly Selective Fluorescent Chemosensor for Iodide in Aqueous Solution. *Org. Lett.* **2007**, *9* (10), 1991–1994.

(30) Mendy, J. S.; Saeed, M. A.; Fronczek, F. R.; Powell, D. R.; Hossain, M. A. Anion Recognition and Sensing by a New Macrocyclic Dinuclear Copper(II) Complex: A Selective Receptor for Iodide. *Inorg. Chem.* **2010**, *49* (16), 7223–7225.

(31) Yawer, M. A.; Havel, V.; Sindelar, V. A Bambusuril Macrocycle That Binds Anions in Water with High Affinity and Selectivity. *Angew. Chem. Int. Ed.* **2015**, *54* (1), 276–279.

(32) Havel, V.; Sindelar, V. Anion Binding Inside a Bambus[6]Uril Macrocycle in Chloroform. *ChemPlusChem* **2015**, *80* (11), 1601–1606.

(33) Zhu, H.; Shi, B.; Chen, K.; Wei, P.; Xia, D.; Mondal, J. H.; Huang, F. Cyclo[4]Carbazole, an Iodide Anion Macrocyclic Receptor. *Org. Lett.* **2016**, *18* (19), 5054–5057.

(34) Langton, M. J.; Marques, I.; Robinson, S. W.; Félix, V.; Beer, P. D. Iodide Recognition and Sensing in Water by a Halogen-Bonding Ruthenium(II)-Based Rotaxane. *Chem. - Eur. J.* **2016**, *22* (1), 185–192.

(35) Li, Y.; Pink, M.; Karty, J. A.; Flood, A. H. Dipole-Promoted and Size-Dependent Cooperativity between Pyridyl-Containing Triazolophanes and Halides Leads to Persistent Sandwich Complexes with Iodide. *J. Am. Chem. Soc.* **2008**, *130* (51), 17293–17295.

(36) Connelly, N. G.; Geiger, W. E. Chemical Redox Agents for Organometallic Chemistry. *Chem. Rev.* **1996**, *96* (2), 877–910.

(37) Ishida, M.; Kim, S.-J.; Preihs, C.; Ohkubo, K.; Lim, J. M.; Lee, B. S.; Park, J. S.; Lynch, V. M.; Roznyatovskiy, V. V.; Sarma, T.; Panda, P. K.; Lee, C.-H.; Fukuzumi, S.; Kim, D.; Sessler, J. L. Protonation-Coupled Redox Reactions in Planar Antiaromatic Meso-Pentafluorophenyl-Substituted o-Phenylene-Bridged Annulated Rosarins. *Nat. Chem.* **2012**, *5* (1), 15–20.

(38) Fukuzumi, S.; Ohkubo, K.; Ishida, M.; Preihs, C.; Chen, B.; Borden, W. T.; Kim, D.; Sessler, J. L. Formation of Ground State Triplet Diradicals from Annulated Rosarin Derivatives by Triprotonation. *J. Am. Chem. Soc.* **2015**, *137* (31), 9780–9783.

(39) Sarma, T.; Kim, G.; Sen, S.; Cha, W.-Y.; Duan, Z.; Moore, M. D.; Lynch, V. M.; Zhang, Z.; Kim, D.; Sessler, J. L. Proton-Coupled Redox Switching in an Annulated π-Extended Core-Modified Octaphyrin. *J. Am. Chem. Soc.* **2018**, 10.1021/jacs.8b06938.

(40) Lee, S.; Mori, H.; Lee, T.; Lim, M.; Osuka, A.; Kim, D. A Very Rapid Electronic Relaxation Process in a Highly Conjugated Zn(II)Porphyrin–[26]Hexaphyrin–Zn(II)Porphyrin Hybrid Tape. *Phys. Chem. Chem. Phys.* **2016**, *18* (4), 3244–3249.

(41) Rose, B. D.; Shoer, L. E.; Wasielewski, M. R.; Haley, M. M. Unusually Short Excited State Lifetimes of Indenofluorene and Fluorenofluorene Derivatives Result from a Conical Intersection. *Chem. Phys. Lett.* **2014**, *616–617*, 137–141.

(42) Borden, W. T.; Davidson, E. R.; Feller, D. The Potential Surface for the Cyclobutadiene Radical Cation. *J. Am. Chem. Soc.* **1981**, *103* (19), 5725–5729.

(43) Lindner, R.; Müller-Dethlefs, K.; Wedum, E.; Haber, K.; Grant, E. R. On the Shape of C6H6+. *Science* **1996**, *271* (5256), 1698–1702.

(44) Kataev, E. A.; Pantos, P.; Karnas, E.; Kolesnikov, G. V.; Tananaev, I. G.; Lynch, V. M.; Sessler, J. L. Perrhenate and Pertechnetate Anion Recognition Properties of Cyclo[8]Pyrrole. *Supramol. Chem.* **2015**, *27* (5–6), 346–356.

(45) Savastano, M.; Bazzicalupi, C.; García, C.; Gellini, C.; Torre, M. D. L. de la; Mariani, P.; Pichierri, F.; Bianchi, A.; Melguizo, M. Iodide and Triiodide Anion Complexes Involving Anion–π Interactions with a Tetrazine-Based Receptor. *Dalton Trans.* **2017**, *46* (14), 4518–4529.

(46) Hausser, K. H.; Brunner, H.; Jochims, J. C. Nuclear Magnetic Resonance of Organic Free Radicals. *Mol. Phys.* **1966**, *10* (3), 253–260.

(47) Kreilick, R. W. NMR Spectra of Some Nitroxide Radicals. *J. Chem. Phys.* **1966**, *45* (6), 1922–1924.

(48) Lang, A.; Naarmann, H.; Walker, N.; Dormann, E. NMR Studies of Stable, Organic Free Radicals. *Synth. Met.* **1993**, *53* (3), 379–398.

(49) Rastrelli, F.; Bagno, A. Predicting the NMR Spectra of Paramagnetic Molecules by DFT: Application to Organic Free Radicals and Transition-Metal Complexes. *Chem. – Eur. J.* **2009**, *15* (32), 7990–8004.

(50) He, L.; Ng, C.-F.; Li, Y.; Liu, Z.; Kuck, D.; Chow, H.-F. Trefoil-Shaped Porous Nanographenes Bearing a Tribenzotriquinacene Core by Three-Fold Scholl Macrocyclization. *Angew. Chem. Int. Ed.* 10.1002/anie.201808461.

(51) Shimizu, D.; Osuka, A. Porphyrinoids as a Platform of Stable Radicals. *Chem. Sci.* **2018**, *9* (6), 1408–1423.

(52) Seidel, D.; Lynch, V.; Sessler, J. L. Cyclo[8]Pyrrole: A Simple-to-Make Expanded Porphyrin with No Meso Bridges. *Angew. Chem. Int. Ed.* **2002**, *41* (8), 1422–1425.

(53) Köhler, T.; Seidel, D.; Lynch, V.; Arp, F. O.; Ou, Z.; Kadish, K. M.; Sessler, J. L. Formation and Properties of Cyclo[6]Pyrrole and Cyclo[7]Pyrrole. *J. Am. Chem. Soc.* **2003**, *125* (23), 6872–6873.

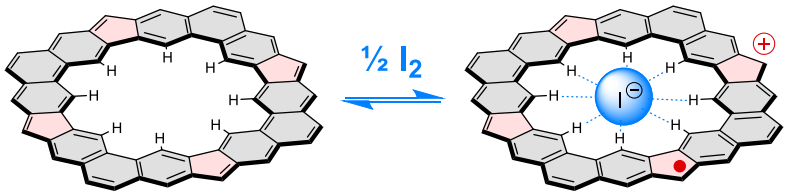
½ I2